# Helicons—The Early Years

Rod W. Boswell and Francis F. Chen

*Abstract*—**Helicon waves are right-hand polarized (RHP) waves which propagate in radially confined magnetized plasmas for frequencies $\omega_{ci} \ll \omega \ll \omega_{ci}$ where $\omega_{ci}$ is the ion cyclotron frequency and $\omega_{ci}$ is the electron cyclotron frequency. They are part of a much larger family of waves which can propagate down to zero frequency and constitute a very rich field for studying complex propagation characteristics and wave–particle interactions. This paper gives a historical perspective of the waves and their relationship to plasma source development up to the mid 1980's, presents a simple description of their propagation characteristics in free and bounded plasmas, and finishes with their first reported use in plasma processing experiments.**

*Index Terms*—**Helicon waves, historical review, plasma sources, wave propagation in cylinders.**

## I. Introduction

THIS paper is the first part of a review of helicon waves and covers the period finishing in the mid 1980's. This date was chosen as it marked the publication of the first experiments on high-density plasma etching using a helicon source; it was also the start of work in this subject at UCLA. Hence, it was natural to divide the major responsibilities of the authors with Boswell taking the early period and Chen taking the subsequent evolution. The present review will naturally follow Boswell's style and his perspective, including, as it does, a certain number of personal opinions. The theoretical development of the dispersion of helicon and whistler waves has been put in the Appendix and only the most basic of equations necessary to clarify the physics of their propagation are presented in the text.

## II. Historical Perspective

The first measurements of right-hand polarized (RHP) waves were apparently made around the second half of the first World War. In order to eavesdrop on telegraphic communications which commonly used single cables and an Earth return, signal corps on opposing sides used to slip out into no-man's land and lay down a few kilometers of cable hoping to pick up the weak currents produced by the telephones. To their great surprise, they picked up considerably more! Clear tones lasting seconds were heard descending in frequency from kHz to hundreds of Hertz. Sometimes these whistling tones were short in duration but repeated many times a second, a sound reminiscent of the dawn chorus of birds. Initially, it was suspected that these were communications from extra-terrestrial beings, and newspapers indulged in some rather fantastic speculation involving messages from Mars.

Manuscript received November 25, 1996; revised August 6, 1997.

R. W. Boswell is with the Plasma Research Laboratory, RSPhysSE, ANU, Canberra, Australia.

F. F. Chen is with the Electrical Engineering Department, University of California, Los Angeles, CA USA.

Publisher Item Identifier S 0093-3813(97)08991-1.

## III. Whistling Atmospherics

The first report in a scientific journal of these whistling tones was given in 1919 by Barkhausen [1] in a paper on new amplifiers applied to magnetometers. Added to this paper was a report of whistling tones from the Earth heard on telephone lines at the war front. They were descending tones from about 1 kHz which lasted up to a second, and sometimes they were so loud that other normal telegraphic communication could not be distinguished. The soldiers christened the phenomenon "the grenades fly," making a sound like "peou." Barkhausen revisited his ideas in 1930 after more was known about the Heavyside layer 100 km above the surface of the Earth, and proposed that a lightning flash could account for the broad frequency spectrum. As for the long duration of the tone, he was at a loss but suggested that the Heavyside layer could induce multiple reflections in the waveguide formed by the earth and the high-altitude reflecting layer.

Actually, the physics of the whistling tones was beyond the then extant knowledge and beyond the Heavyside layer.

The following two years brought papers by Hartree [2] and Appleton [3] who, following a physical and engineering viewpoint, respectively, developed the first theory for the propagation of electromagnetic waves in a magnetized plasma. The need for such a theory was driven by a critical social desire, *viz.*, the wish to communicate over large distances without using wires, and the radio waves in use showed dramatic fluctuations in reception depending on the frequency and the time of day. They obtained an equation for the refractive index which depended on the plasma density, magnetic field, frequency, and propagation angle. Three years later, Booker [4] simplified the relatively cumberson Appleton–Hartree dispersion relation into quasilongitudinal and quasitransverse wave propagation cases (relative to the magnetic field) yielding, for the waves we are interested in, the rather simple dispersion relation

$$N^2 = 1 - \frac{\omega_{pe}^2}{\omega(\omega - \omega_{ce}\cos\theta)} \tag{1}$$

where

- $N$ refractive index of the plasma defined as the ratio of the speed of light to the phase velocity ($v_\phi = \omega/k$) of the wave;
- $\omega_{pe}$ electron plasma frequency;
- $\omega_{ce}$ electron cyclotron frequency;
- $\theta$ angle between the wave vector ($k$) and the magnetic field ($B_o$).

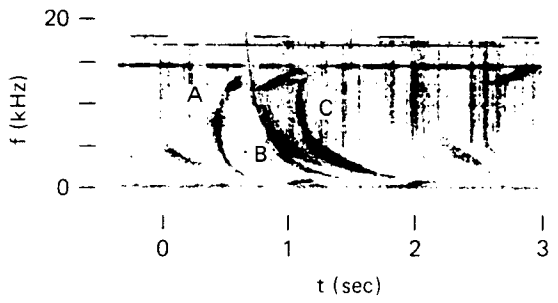


Fig. 1. Spectrogram of whistler signals showing the descending tones (increasing darkness is proportional to signal strength) as a function of time. Curve A is a "nose" whistle with simultaneous rising and falling tones and curve B shows a more characteristic continuous descending glide tone. (Reprinted from D. L. Carpenter, *J. Geophys. Res.*, vol. 71, p. 693, 1966.)

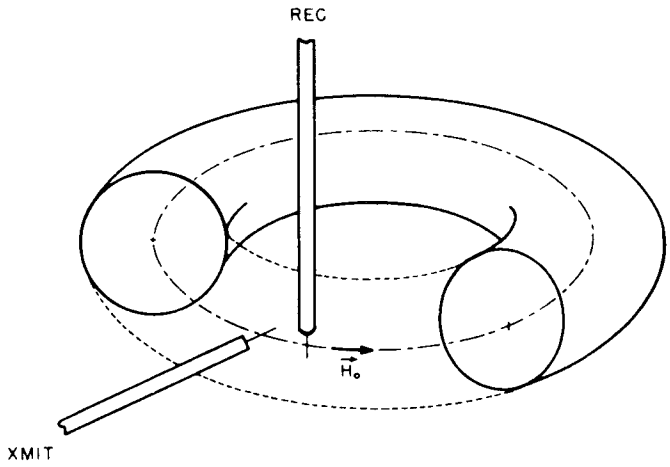


Fig. 2. Cartoon of the ZETA experiment showing the transmitting and receiving antennae. (Reprinted from [14].)

It is clear that for $k$ parallel to $B_o$, $N$ goes to infinity as $\omega$ approaches $\omega_{ce}$, giving rise to the electron cyclotron resonance. The existence of the $\cos\theta$ in the denominator shows that the refractive index is anisotropic and that resonances will occur when $\omega$ is less than $\omega_{ce}$ for waves propagating off axis. In this case, the group velocity vector has to be considered and this was demonstrated by Storey [5] in Cambridge who simplified (1) by considering low frequencies and high refractive indexes to obtain

$$N^2 \approx \frac{\omega_{pe}^2}{\omega\omega_{ce}\cos\theta}. \tag{2}$$

From (2) he deduced that the maximum angle for the group velocity vector must be less than 19°28′. Hence, the whistlers are constrained to propagate at angles close to the direction of the magnetic field. Further analysis showed that the group velocity had a maximum at $1/4\omega/\omega_{ce}$, so frequencies lower and higher than this would travel slower and would arrive at an observer later. These two phenomena—the lightning strike providing a point source with a broad frequency spectrum and the anisotropic dispersive plasma—provided the explanation for the whistling atmospherics and have been used subsequently as a diagnostic for the equatorial magnetic field deep in the Earth's magnetosphere along the field line guiding the whistler. Examples of magnetospheric whistlers are shown in the ionogram of Fig. 1 where the descending tones lasting about one second are clearly visible. The trace "A" is called a nose whistler, the simultaneous rising and falling tone arising from the frequency dependence of the group velocity. This particular whistler has a nose frequency (maximum group velocity) of about 8 kHz, showing us that it was ducted along a magnetic field line which had a minimum value of 3 mG in the equatorial magnetosphere at an altitude of 4–5 $R_e$ (an Earth radii $R_e$ = 6000 km). These ideas will be developed further in the theory section of this paper as they have direct relevance to helicon sources.

## IV. Development of Basic Wave-Particle Processes

The period following the explosion of the atomic bomb marked the beginning of plasma physics as a major field of study internationally. Initially, it was the fusion bomb and later the search to create controlled fusion energy which provided the impetus (and the generous funding) for the research on wave propagation in experimental laboratory plasmas, whence came the development and understanding of contemporary helicon sources.

Apart from the p ropagation characteristics of the wave, which are well described by (2), the major interest in helicon waves is how the energy of the wave is transferred to the plasma, that is, is it possible to use the wave to create a plasma? Strangely enough, plasmas are the only state of matter in which dissipation of energy can occur without collisions. This phenomenon was discovered by Landau in 1946 [6] in the course of a rigorous solution of the Vlasov equation (which describes the interaction of charged particles with the electric and magnetic fields of a collisionless plasma). The physical mechanism was elucidated some 15 years later by Dawson [7] who showed that charged particles with a velocity close to the phase velocity (not the group velocity) of a wave suffer a net gain of energy at the expense of the wave which consequently decreases in amplitude. This phenomenon has been dubbed "Landau damping," and further will be said of this later in the paper.

## V. Helicons in Solid-State Plasmas

The name "helicon" was suggested by Aigrain in 1960 [8] to describe an electromagnetic wave which propagates in solid metals at low temperatures with frequencies between the electron and ion cyclotron frequencies. These waves were initially observed as resonances or standing waves in sodium at liquid helium temperatures [9] and until 1964 the plane-wave dispersion relation (2), modified by geometrical factors, was used to explain the experimental results. In 1964, Legendy [10] in the United States and Klosenberg, McNamara, and Thonemann (KMT) [11] in the United Kingdom independently presented theories for the propagation of helicon waves in cylindrical magnetoplasmas. Both papers present effectively the same theoretical treatment and speculate on the zero-resistivity case with vacuum boundaries, but KMT also presented calculated dispersion and attenuation curves. These theoretical predictions were in good agreement with experiments carried out in low-temperature indium by Harding and Thonemann, [12] as well as Facey and Harding [13]. A

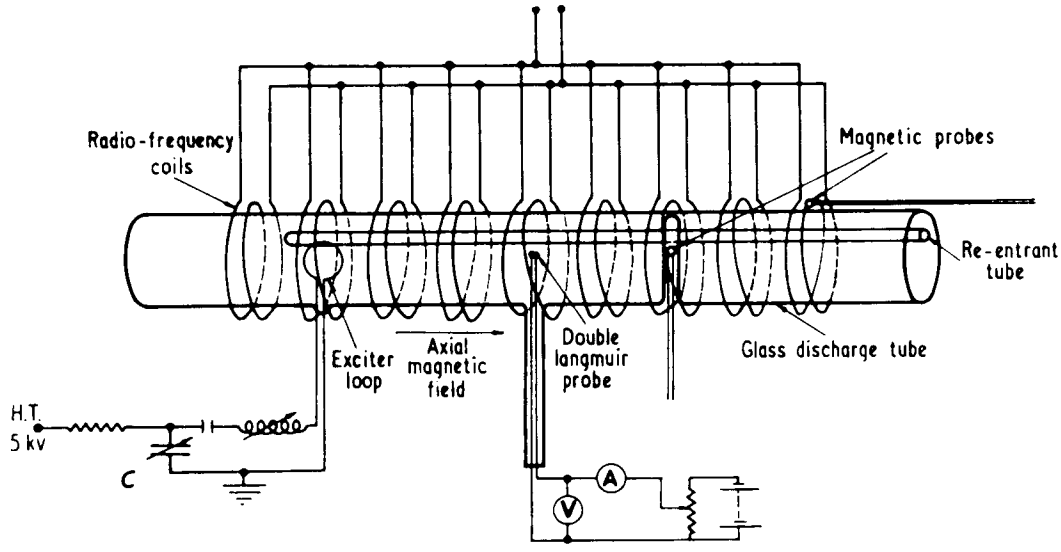


Fig. 3. Schematic diagram of the L & T experiment. Note the plasma is created by the distributed antenna of nine sets of double loops and the waves are launched by a separate exciter loop powered by a tuned circuit at high voltage discharging through a spark gap. (Reprinted from [16].)

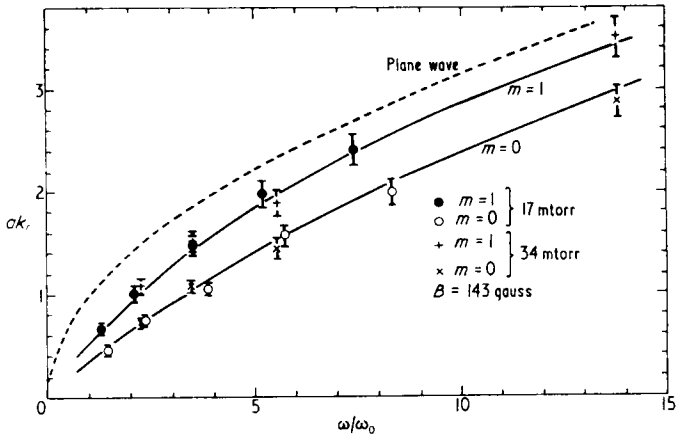


Fig. 4. Dispersion of $m = 0$ and $m = 1$ test waves compared to the theory of KMT and the infinite plane-wave dispersion. (Reprinted from [16].)

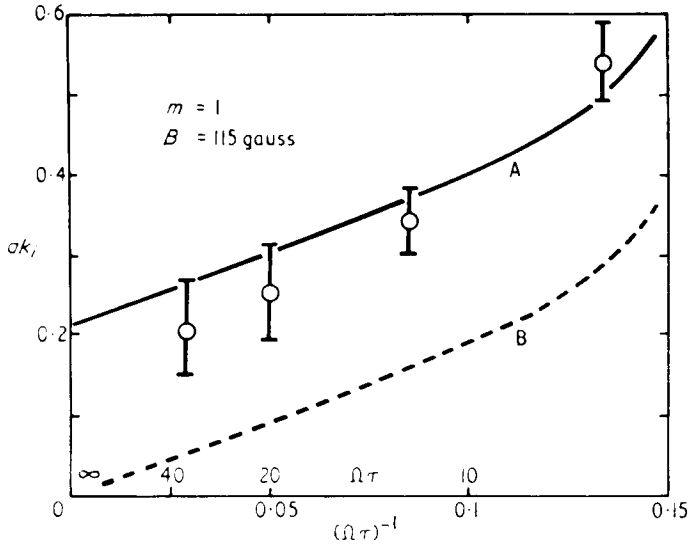


Fig. 5. Variation of the wave damping as the collision parameter ($\Omega\tau = \omega_{ce}/\nu$ where $\nu$ is the collision frequency) is varied for a constant wavelength ($ak_r = 0.68$). Theoretical curve A was obtained by including the vacuum fields outside the glass vacuum vessel and curve B by neglecting the vacuum fields. These results clearly show the importance of choosing the correct boundary conditions. (Reprinted from [16].)

considerable amount of further work has been done in solid-state physics on these helicon resonances which is not directly relevant to helicon sources, so our subsequent discussion will be limited to gaseous plasmas.

## VI. Helicons in Gaseous Plasmas

The first observation of this wave mode in gaseous plasmas [14] was carried out in ZETA, a large toroidal experiment for fusion research, where the guiding of the wave along the magnetic field lines was reported in 1960. The toroidal geometry and the transmitting and receiving antennae are shown in Fig. 2. Shortly after, Blevin and Thonemann [15] used a rotating magnetic field to transfer energy to the electrons, which rotated producing an azimuthal current. The axial magnetic field produced by this current was opposite in direction to the applied magnetic field and acted as a plasma-confining mechanism (minimum B). A high-frequency oscillation seen on magnetic probe signals was thought to be a standing helicon wave produced by the applied oscillating fields. The first experiment aimed specifically at studying helicon-wave propagation using low-amplitude test waves was conducted by Lehane and Thonemann [16] in a cylindrical RF-maintained plasma. A diagram of their apparatus is given in Fig. 3, and it consists of a glass tube 10-cm diameter and 100-cm long, axial $B_o < 500$ G, a pressure of xenon gas from 10–70 mTorr, and a 3 kW RF generator operating at about 15 MHz. The plasma was excited by an antenna structure containing nine two-turn coils wound around the glass cylinder and equally spaced along it. Although they used the RF generator simply to create the plasma, the antenna structure was periodic and may well have launched helicon waves as well.

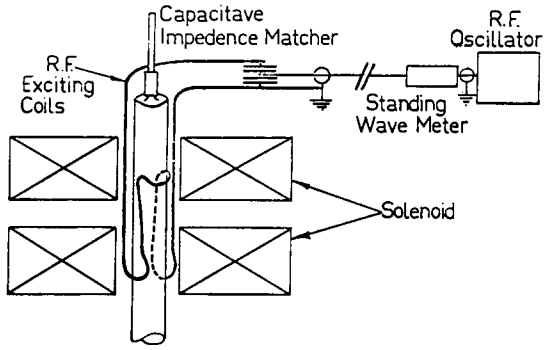


Fig. 6. The small Flinders apparatus showing the first drawing of the double saddle field antenna.

Average electron densities ranged from 3–5 $\times$ $10^{12}$ $cm^{-3}$ and electron temperatures of 25 000–15 000 K were measured over this increasing pressure range. Both $m = 0$ and $m = 1$ test waves were launched from small antennae at various frequencies and their dispersion compared favorably with the theory of KMT (Fig. 4). The importance of the vacuum fields, which exist outside a plasma with insulating boundaries, on the wave damping was also measured and is shown in Fig. 5.

The above experiments were carried out at sufficiently high pressures that the wave damping could simply be explained by electron-neutral collisions. For low-collision frequencies, a number of problems associated with the plasma–insulator gap at the radial boundary and the wave dissipation arise. The resonant heating of a plasma at the low-frequency end of the helicon regime was described by Chechin *et al.* in 1965 [17] and more fully investigated by Vasil'ev *et al.* in 1968 [18]. The anomalously high damping encountered was initially thought to be due to Cherenkov (Landau) damping [19], but later measurements showed that the linear theory could not be applied. The anomalous skin effect (a type of collisionless transit time damping) was investigated to see whether it had an effect on the dispersion and damping of helicons [20], [21].

## VII. Australian Helicon Source Experiments

### A. Small-Diameter Experiments

Further experiments were carried out by Blevin when he returned to Australia from the United Kingdom in the mid 1960's, first at the University of New England in New South Wales and from 1967 at Flinders University in Adelaide, South Australia. These used low-pressure mercury arc columns and the dispersion of $m = 1$ and $m = 0$ azimuthal waves were studied with antennae immersed in the plasma column. Radial density gradients were shown to have a major effect in a plasma with conducting walls and confidence in the theory was such that helicons were used as a plasma diagnostic [22]–[25].

During this period at Flinders, Boswell was trying to measure ion cyclotron waves (the left-hand polarized wave mode) in a $J \times B$ shock-produced plasma, and it became evident in 1968 after a couple of years of research that a far less collisional plasma would be required. Following discussions with Christiansen (who was finishing his Ph.D. thesis with Blevin at the time), it was decided that it should be possible to excite a helicon wave using a simple transverse high-frequency

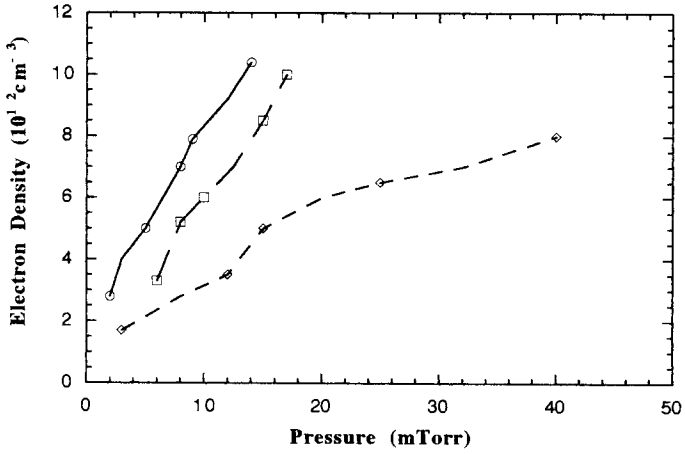


Fig. 7. Electron density in the small Flinders machine as a function of pressure for three magnetic fields (solid line 1150 G, large dashes 2000 G, small dashes 400 G).

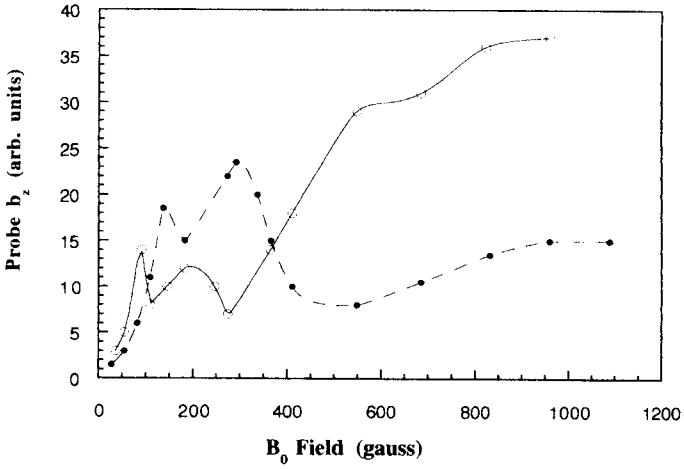


Fig. 8. Plasma "wave" fields ($B_z$) as the axial magnetic field is varied for two pressures (solid line 9 mTorr, dashed line 27 mTorr). Note the apparent resonances which change with the pressure.

field, similar to that described by Blevin and Thonemann [15]. The experimental apparatus is shown in Fig. 6 and consisted of a 5-cm-diameter 55-cm-long glass tube attached to a vacuum system and inserted into two magnetic field coils ("borrowed" from the second-year laboratory) capable of producing a field of 2 kG. The gas used was argon and the RF generator was pulsed with a period of 100 ms and a duty cycle of 10% for frequencies from 6–28 MHz.

The antenna can be seen in Fig. 6 and was fabricated from a single piece of copper wire bent to form two loops approximately 16 cm long carrying the RF current in the same direction on either side of the glass tube between the two solenoids. Two sections of the wire continued up through the top solenoid and were connected to the capacitive matching network. Earlier theoretical analysis and experimental measurements in the mercury plasma at Flinders had shown that the radial magnetic field of the $m = 1$ helicon mode was continuous across the plasma–glass interface and extended outside the glass vacuum tube. Hence it was thought that the transverse RF field created by the pair of loops could couple

with the plasma fields and launch a helicon wave. Additionally, if the antenna was half a wavelength long it should be possible to resonantly excite the helicon. From (2) it was clear that the plasma density needed to be known and the resonance condition would depend on both the RF frequency and the magnetic field.

The electron density ($n_e$) was measured in between the solenoids with a 35-GHz interferometer having a cutoff $n_e$ of about $10^{13}$ cm$^{-3}$. The initial experiments varying the frequency showed that $n_e$ had a broad maximum of about $3 \times 10^{12}$ cm$^{-3}$ at 8.5 MHz, with no magnetic field and a pressure of 38 mTorr. In Fig. 7, the variation of $n_e$ with pressure is shown for three different magnetic fields. There was clearly a maximum at a field somewhere between 400 and 1150 G and, although the interferometer was cutoff at 38 mTorr, we can estimate that for the optimum field, $n_e$ would have been approximately $3 \times 10^{13}$ cm$^{-3}$, ten times greater than that measured without the magnetic field. The plasma color was an intense blue, too bright to observe directly with the eye. Additionally, the blue central column (which maintained its diameter of about 1 cm) extended 10–20 cm beyond the end of the top solenoid and did not expand with the magnetic field. Where the column struck the glass top of the vacuum tube, the glass became red hot and melted over a period of a minute or so! Subsequent tubes were made considerably longer.

To measure the RF magnetic field in the plasma, a small search coil was constructed and inserted radially into the plasma between the two solenoids and oriented to measure the $B_z$ component at a distance of 1.5 cm from the center, where the theory predicted a maximum. The amplitude of the signal from this probe is shown in Fig. 8 for 9 and 27 mTorr as the axial magnetic field was increased. Two maxima can be seen for low magnetic fields and the magnetic fields corresponding to these maxima increases linearly with pressure suggesting some form of resonant behavior. An approximate calculation using (2) for the second maxima at 9 mTorr yielded a wavelength of between 20 and 30 cm. This was considered to be strong evidence for the existence of a helicon wave in the system, and a second larger system was constructed to allow more detailed measurements to be made. These measurements were made over a period of a few months in 1968, but their importance was not obvious at the time so they only exist as an internal report [26]. The experimental results from the large tube were subsequently published [27], [28] and a brief review is given here.

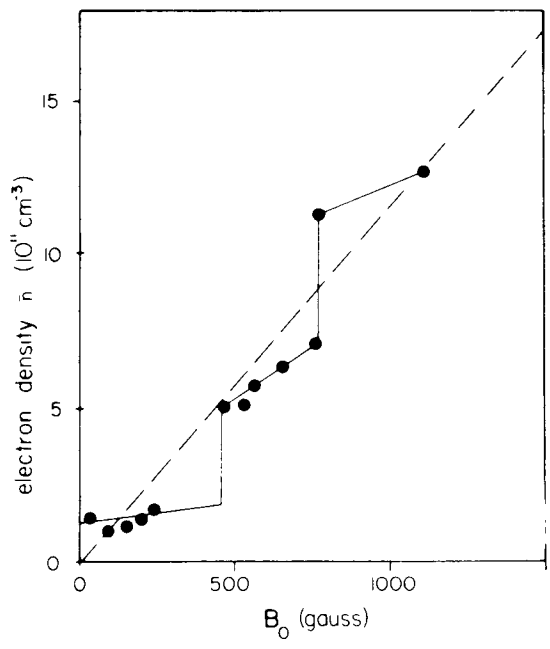


Fig. 9. Electron density in the large Flinders apparatus as a function of $B_0$ showing the density jumps. The dashed line is the theoretically expected dispersion for a helicon wave excited with a wavelength twice that of the antenna.

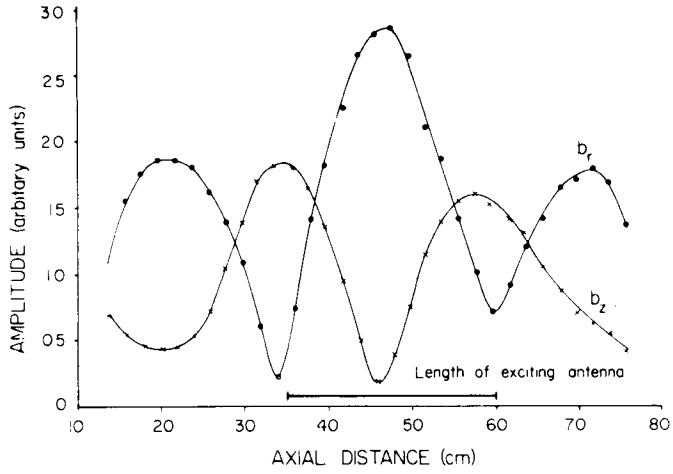


Fig. 10. Axial variation of $B_r$ and $B_z$ in the large Flinders machine for $B_0 = 100$ G. The waves are stationary with phase changes of $\pi$ at each minimum.

## VIII. The Large-Diameter Tube

The general arrangement is similar to Fig. 6 except the dimensions—the pyrex glass tube was 120 cm long 10-cm diameter sealed at one end, while the other end was connected to the diffusion pump and the gas inlet to minimize pressure gradients along the axis. All measurements were made with a pressure of 1.5-mTorr argon, a RF of 8.6-MHz, and a power of 180 W.

Four solenoids provided a magnetic field of up to 1.6 kG, uniform to ±5% over an axial distance of 60 cm. The antenna was of the double-loop structure discussed above and was fabricated from 1-cm-wide strips of copper with the feed to the matching network located in the center rather than at the ends to prevent the end effects observed in the small tube.

Small magnetic field probes (B dot probes) could be inserted axially or between the central two solenoids to measure the $r$, $\theta$, and $z$ components of the wave fields, both radially to determine the mode structure and axially to determine the axial wavelength. Considerable care was taken to position the radial probes exactly midway between the two axial strips of the antenna which carried current in the same direction so that direct pick up of the antenna fields was minimized. Maximum wave fields of 1 G were obtained for $B_0 \sim 1$ kG.

Relative measurements of the electron density were made with a double Langmuir probe oriented along $B_0$ and used

with the line densities across a diameter made with the 35-GHz interferometer to obtain absolute radial density profiles. The density increase with $B_0$ is given in Fig. 9. The jumps, observable at 450 and 750 G, were only obtained by dramatically changing the match-box tuning; if this were kept constant for a good standing wave ratio (SWR) in the generator/match-box coax at $B_0 \sim 50$ G and then the $B_0$ increased, the density would remain reasonably constant but the SWR would increase to values well over three. The dashed line in Fig. 9 is the theoretical result for plane-wave propagation (2) which reduces to

$$n \sim 1.2 \times 10^9 B_0 \text{ cm}^{-3} \tag{3}$$

for an imposed wavelength of 50 cm, i.e., twice the antenna length. The axial variations of the wave $B_r$ and $B_\theta$ are shown in Fig. 10 for $B_0 = 100$ G where it can be seen that the $B_r$ component fits well with the imposed transverse field created by the antenna. Phase measurements along the axis showed the wave to be a standing wave under the antenna and radial measurements defined the wave to be an $m = 1$ mode. Caution must be used with fitting the axial wavelength measurements as these were made under the antenna and showed variations of up to 50% outside this region. Basically, the system is a forced resonator with its major defining parameter $n_e$ being nonlinearly dependent on the input parameters.

The increase in density with $B_0$ was associated with a narrowing of the plasma column, from a full width half maximum of 5 cm at 37 G to 2 cm at 1130 G. Although the decrease in the cross-field diffusion could account for an increase in the peak density of a factor of about six (with the average density remaining the same), it is the average density which increases by a factor of about ten implying that the helicon wave is profoundly involved in the ionization of the plasma.

A numerical method for solving (A14) in cylindrical coordinates (developed by Davies, which allowed for radial density gradients [52]) was modified to include the effects of rigid nonconducting boundaries and standing rather than propagating waves. It was found that an effective resistivity, about 1000 times that given by simple collisions, was necessary to fit the radial wave field profiles. Using the theoretical value produced solutions with large fields constrained to a narrow layer at the surface of the plasma which propagated into the plasma a distance of about the collisionless skin depth. Theoretical research by a number of groups in the 1990's appears to suggest that these large fields may be associated with TG modes (see the Appendix).

The very high value of the effective resistivity was a puzzle, and considerable time was spent searching the literature for possible collisionless mechanisms. Using a theory developed by Shafranov [29] and Dolgopolov [30] for Cherenkov damping (as the presently known Landau damping was apparently known in the USSR at the time) in a cylindrical plasma it was shown that, for the conditions of this experiment, Cherenkov damping was ten times greater than collisional damping but, unfortunately, still 100 times smaller than that required to explain the experimental results. "Plus ça change, plus c'est la meme chose." Although this discussion constituted a chapter of Boswell's thesis, it was clear that under these experimental conditions, the simple linear derivations of Landau or Cherenkov damping were not adequate in explaining the experimental results.

## IX. The Development of Similar Systems

Experiments on electron cyclotron wave resonances were being conducted in the late 1960's in West Germany by Oechsner [31]–[33] in a glass cylinder 9 cm in length and diameter. In this case, however, the magnetic field of up to 50 G was perpendicular to the tube axis and the antenna was a single loop surrounding the cylinder. Resonances similar to those of Fig. 7 were observed for RF of 27 MHz and 2 kW and interpreted as being cavity resonances ($\lambda/2$, $3\lambda/2$, etc.) of waves with $\omega/\omega_{ce} \sim 0.25$. The electron density was enhanced during the resonances and a theory was developed linking electron heating in the high electric fields of the resonance to the increased ionization.

It is not possible to proceed further without mention of the "Lisitano" coil [34] which is a slotted slow-wave antenna operating in the gigahertz range of frequencies. Although it is commonly thought of as an electron cyclotron resonance (ECR) source, it was able to produce long columns of highly ionized plasma when operating with $\omega \sim 0.5\omega_{ce}$, i.e., at the maximum phase velocity of the whistler wave. Modern ECR sources operate under similar conditions.

We will now make a distinction between antennae which were designed to launch waves in the helicon region and the experiments above which were specifically designed to look at the ionization of a background gas by helicon waves.

The bibliography of the former is immense and concerns wave launching experiments on fusion devices for particle heating rather than ionization, in particular, the heating of ions. The antenna structure normally follows the design developed by Stix [45] for launching ion cyclotron waves and compressional Alfven waves (which are low-frequency helicon waves). This antenna consisted of current loops wound outside the insulating vacuum tube with their axis parallel to the tube axis. These were spaced in groups along the tube, separated by 1/2 wavelength of the desired wave with their current direction reversed for every other group. The idea was to resonantly launch $m = 0$-mode waves. The simplest form of the antenna is called a $M = 1$. $N = 1$ consisting of two single-turn loops with opposed currents separated by 1/2 wavelength.

Another type commonly used was the helical antenna [34] which could be used to launch either $m = +1$ or $m = -1$ modes depending on the symmetry and the direction of the magnetic field. This form of antenna was also used at the University of Sussex in the early 1970's to create a helicon plasma quite successfully, its main disadvantage is that the multi-turn spiral has quite a high $Q$ and consequently only one optimum operating condition. Finding it can frustrate the most patient student.

Many experiments were carried out in the 1970's on lower hybrid heating, fast wave heating and current generation, and a variety of low-frequency Alfven wave heating schemes. Of interest to this review is a paper published by a large number

of researchers in the Nagoya group [36] on "Radio-frequency plugging of a high-density plasma" which showed for the first time the Nagoya type III antenna. The type I was the simple helix and the type II was a form of double half turn with the current up one side and down the other (apparently). In essence, the type III is a simplification of the double-loop (or double-saddle field) antenna used earlier [37]; both produce an oscillating RF field transverse to the axial magnetic field and both have an axial length appropriate to 1/2 wavelength of the required helicon wave. The first report on using this type of antenna for plasma production was in 1986 by Shoji in the Annual Review of the Nagoya Institute of Plasma Physics [38] and the first publication was sometime later [39]. This, however, is somewhat in the future of our present review and we return to the early 1980's.

## X. Helicon Experiments at the ANU

In 1980, the basic design of a 20-cm-diameter helicon source attached to a 100-cm-diameter diffusion chamber was defined and the completed apparatus Waves on Magnetized Beams and Turbulence (WOMBAT) commissioned in 1981. Its purpose was to simulate wave and electron beam interactions with the Auroral plasma. During its construction, a small system of 5-cm diameter with a magnetic field up to 4 kG was put together to repeat the early experiments on the small tube experiment at Flinders. This was carried out in collaboration with the University of Orleans (France) which had a similar system. The diagnostics were mainly optical emission spectroscopy (as it was thought that it may be possible to create an argon ion laser), and a 90-GHz interferometer which allowed average densities up to about $10^{14}$ cm$^{-3}$ to be measured across a diameter. For input powers of 1 kW at 7 MHz to a center fed double-loop antenna, average densities of $0.5–0.8 \times 10^{13}$ cm$^{-3}$ were obtained for argon pressures of a few milliTorr [40]. Radial intensity profiles of ArI were hollow while those of ArII were peaked strongly in the center with a FWHM of about 1 cm, implying that the central plasma density was around ten times the line average across a diameter. As the magnetic field was increased, the ArII line had a minimum FWHM and a maximum intensity at about 1 kG. Further increasing the field resulted in a decrease in the ArII line and an increase in the ArII line until at 3.5 kG it was estimated that the plasma was not only fully ionized, but also consisted of at least 50% $Ar^{++}$ ions. The neutral temperature was about 0.5 eV and the ion temperature 1 eV. The discharge was shown to be in a simple corona equilibrium and, as it was fully ionized, radiation losses from the ArII and ArIII transitions to the ground state limited the electron temperature to 3 eV.

As happens quite often in the development of a new technology, the step into etching involved a change in research area of a close colleague. In this case it was a researcher, Daniel Henry, in French Telecom (CNET) who was transferred from the space physics department in Orleans (close to the university) to a new center for microelectronics development in Grenoble. The ANU had, and still has, close collaborative links with French research groups in Orleans, Nantes, Grenoble, and Paris, and this allowed Henry to spend a month

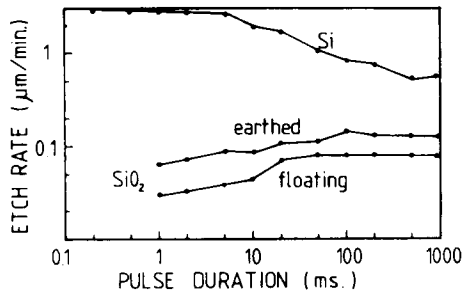


Fig. 11. Etch rates for Si and $SiO_2$ with $SF_6$ for earthed and floating sample holders as a function of the pulse duration (on time) for a duty cycle of 20% in the small high-density BASIL device at the ANU. (Reprinted from [41].)

in 1984 in Australia. He brought with him some early 4-in CMOS test wafers (aluminum mask, 0.5-$\mu$m polysilicon, and 0.1-$\mu$m thermal oxide on bulk crystal silicon) to test etching characteristics in the small high-density machine (BASIL) and in WOMBAT. There was rather a paucity of information of etching in high-density plasmas at this time, although some tests had been carried out in ECR systems in France. Armed with the courage of ignorance, Boswell and Henry [41] made the first experiments with small samples of 1 cm$^2$ in BASIL using a $SF_6$ plasma having a peak density of above $10^{13}$ cm$^{-3}$ produced by 7-MHz RF at 500 W pulsed on for 100 ms. with a duty cycle of 20%. The initial experiments were carried out with pressures around 1 mTorr, and no etching was observed in spite of strong FII emission being observed. The pressure was then increased up to 7 mTorr and the etch rates measured with a simple He/Ne interferometer were depressingly low at about 0.2 $\mu$m min$^{-1}$. There was, however, a rather noisy signal at the beginning of the etch which was initially thought to be a vibration problem. It turned out, on reflection, that the noise was in fact a real measurement of the polysilicon etch with fast fringes due to the high refractive index of silicon followed by the slower fringes formed by reflections from the mask and the bottom of the etched area. Once this was realized, the real etch rate, corrected for the refractive index of air, was calculated at about 0.8 $\mu$m min$^{-1}$. Keeping the duty cycle constant and increasing the pulse frequency showed a remarkable increase in the Si etch rate to 3 $\mu$m min$^{-1}$. At the same time, the oxide etch rate decreased by more than a factor of two. These results are shown in Fig. 11. Biasing the substrate holder at 100 V with a second generator increased the oxide etch rate somewhat but did not change the Si etch rate. Allowing the substrate to heat from 20 to over 100°C did not change the etch rate.

The results were explained by proposing that etching continued in the afterglow for a period of up to 50 ms after the RF was pulsed off and the plasma density had decayed by many orders of magnitude. The only mechanism possible was the etching of the Si by atoms of fluorine which would have a lifetime determined by recombination to the fluorine molecule on the passivated walls of about 50 ms. There were a number of important implications for the conditions of this experiment.

- Very high etch rates of Si by $SF_6$ could be obtained at low pressure.

- For pulse frequencies around 1 kHz, RF power at 20% duty cycle gave the same etch rate for Si as for continuous power.
- The etch rate seemed to be limited by the thermal flux of fluorine to the surface without any activation energy being apparent.
- Etching continued in the afterglow at a rate determined by the atomic fluorine density.
- The $Si/SiO_2$ selectivity could be improved by increasing the pulsing frequency.

Following these experiments, it was decided to patent the association of a helicon source with a diffusion chamber [42]. At the time these experiments were being carried out, Chen spent a three-month sabbatical period with the plasma group at the ANU and became fascinated with the high plasma densities which could be generated with a helicon wave, and on returning to UCLA started the first experiments in the United States. The period from 1984 to the present will be discussed in "Helicons, the Past Decade" (this issue, pp. 1245–1257), as will details of the experimental results from WOMBAT and subsequent plasma processing systems developed at the ANU.

## APPENDIX

As the nomenclature of the many types of waves which can exist in a magnetized plasma is perhaps somewhat confusing, here we give a simple introduction to wave propagation using the variation of the square of the refractive index with frequency to delineate the different modes and their names. We will neglect thermal effects, which means that there is no pressure term and hence no ion or electron acoustic waves. A resonance occurs when the wave phase velocity decreases to zero causing the refractive index to go to infinity, and a cutoff when the refractive index goes to zero. Negative values of the square of the refractive index mean that the phase velocity is purely imaginary and there is no real value of the wavelength. The wave is then evanescent.

### *A. Propagation of Waves Parallel to the Magnetic Field in an Infinite Uniform Plasma*

There are a variety of ways to investigate wave propagation in plasmas. We have chosen to follow Spitzer [43] The hydromagnetic approximation of the "generalized Ohms Law" for a plasma can be written

$$\frac{m_e}{ne^2}\frac{\partial J}{\partial t} = E_1 + V \times B + \frac{1}{ne}\nabla P_e - \frac{1}{ne} J \times B - \eta J \quad \text{(A1)}$$

where

$m_e$ electron mass;
$n$ charged-particle density;
$e$ electronic charge;
$j$ current density;
$E_1$ electric field;
$B$ magnetic induction;
$V$ plasma velocity;
$P_e$ electron partial pressure;
$\eta$ plasma resistivity = $m_e/ne^2\tau$;
$\tau$ electron-neutral collision time.

Assuming $\underline{E}_0$, $\underline{J}_0$, $\underline{V}_0$, and $\underline{B}_0$ are the values of $\underline{E}_1$, $\underline{J}$, $\underline{V}$, and $\underline{B}$ in the unperturbed plasma, and $\underline{E}$, $\underline{j}$, $\underline{v}$, and $\underline{b}$ are perturbations due to the wave, then to the first order, (A1) can be written for perturbing quantities, assuming no steady currents flow as

$$\frac{m_e}{ne^2}\frac{\partial j}{\partial t} = \underline{E} + \underline{v} \times \underline{B}_0 - \frac{1}{ne}\underline{j} \times \underline{B}_0 - \eta j. \quad \text{(A2)}$$

The pressure gradient has been dropped in (A2) on the assumption of a cold plasma.

Using Cartesian coordinates with the steady applied magnetic field in the $z$-direction, the linearized equation of motion for a plasma, Maxwell's equations for perturbed quantities, and perturbations of the form

$$f = \text{const} \exp i(\omega t - kz)$$

where $\omega$ and $k$ are the angular frequency and wave number of the wave, respectively. Some algebra yields

$$\left(\frac{k}{k_0}\right)^2\left(1 + \frac{\omega_{ci}}{\omega} - \frac{\omega}{\omega_{ce}} - \frac{i}{\omega_{ce}\tau}\right) = \frac{1}{(1 - v^2/c^2)} \quad \text{(A3)}$$

where

$$(k_0)^2 = \frac{ne\omega c^2}{\varepsilon_0 B_0}$$

for plane-wave propagation.

Terms in (A3) can be identified with terms in the initial formulation [44] and may be ignored in the following circumstances.

1) $v^2/c^2$ corresponds to the displacement current term in Maxwell's equation and can be ignored if the wave velocity $\ll$ velocity of light.
2) $i/\omega_{ce}\tau$ corresponds to $\eta$ and is neglected if the electron–cyclotron frequency $\omega_{ce} \gg \nu$, the collision frequency for electrons and neutrals.
3) $\omega_{ci}/\omega$ corresponds to the $\underline{v} \times \underline{B}$ and can be ignored if $\omega \gg$ ion–cyclotron frequency $\omega_{ci}$.
4) $\omega/\omega_{ce}$ corresponds to the electron inertial term and can be ignored if a) $\omega \ll \omega_{ce}$ and b) the plasma density is high.

Introducing the plasma frequency $\omega_{pe} = (ne^2/\varepsilon_0 m_e)^{1/2}$ and considering the case of zero resistivity, (A3) can be rearranged as

$$N^2 = \frac{k^2c^2}{\omega^2} = \frac{\omega_{pe}^2}{\omega_{ce}\omega\left(1 - \dfrac{v^2}{c^2}\right)\left(1 + \dfrac{\omega_{ci}}{\omega} - \dfrac{\omega}{\omega_{ce}}\right)}. \quad \text{(A4)}$$

The dispersion of the wave modes resulting from this equation is sketched in Fig. 12 for $\omega_{pe} \gg \omega_{ce}$. There are always two solutions to the quadratic, below $\omega_{ci}$, both modes (the left and right-hand polarized) are real and merge at very low frequencies to form the Alfven wave. The left-hand polarized wave rotates in the same direction as the ions and has a resonance at $\omega_{ci}$, becoming evanescent above this frequency. The right-hand polarized wave rotates in the same direction as the electrons, resonating at $\omega_{ce}$ and becoming evanescent above $\omega_{ce}$. Both modes become real again at the left and right cutoff frequencies which straddle and are close to $\omega_{pe}$. As

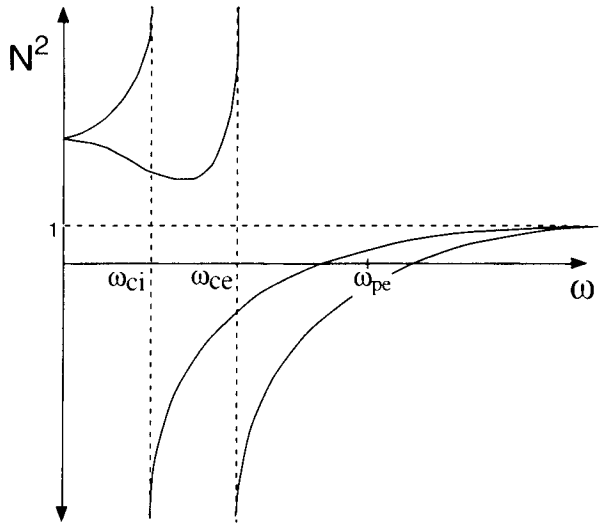


Fig. 12. Sketch of the dispersion of the LHP and RHP waves propagating parallel to the magnetic field for $\omega_{pe} \gg \omega_{ce}$.

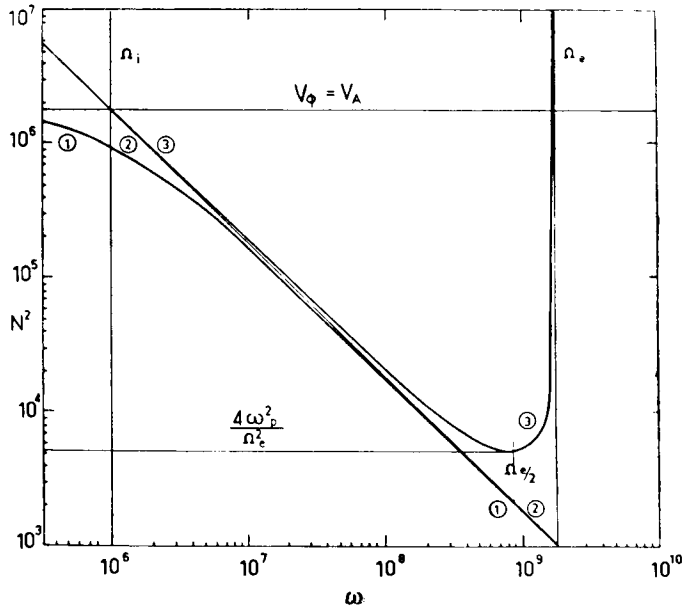


Fig. 13. Dispersion of the RHP wave between the ion and electron cyclotron frequencies. Curve 1 is the compressional or fast Alfven wave, curve 2 is the Helicon wave, and curve 3 is the electron cyclotron wave. Helicons (or whistlers) must often be characterized by using both the Hall term and the electron inertia. Conditions are hydrogen plasma, $B_0 = 100$ G, and a plasma density of $10^{12}$ cm$^{-3}$.

the frequency further increases, they asymptotically approach the speed of light from above. The small difference in the dispersion gives rise to the Faraday effect, a useful diagnostic in plasmas. In further discussion, we will only consider real waves with velocities much less than the velocity of light.

### *B. The Right-Hand Polarized Wave Below the Electron-Cyclotron Resonance*

The three regions of different approximation to the Ohms Law, depending on the relative magnitude of the frequencies $\omega_{ci}$ and $\omega_{ce}$, are set out below for $\omega_{pe} \gg \omega_{ce}$ and $v \ll c$.

*1) Compressional Alfven Waves:* In this regime, the electron inertia is neglected and the term $\omega/\omega_{ce}$ is dropped out of (A4). The equation describing the dispersion of these waves is

$$N^2 = \frac{\omega_{pe}^2}{\omega_{ce}\left[\omega_{ci} + \omega\right]} \tag{A5}$$

when $\omega \ll \omega_{ci}$

$$N^2 = \frac{\omega_{pe}^2}{\omega_{ci}\omega_{ce}}$$

and the phase velocity of the wave becomes

$$V_\phi = \frac{c}{N} = \frac{c}{\omega_{pe}}\sqrt{\omega_{ci}\omega_{ce}} = V_A$$

the Alfven velocity. The compressional wave can be seen to arise from a combination of the $\underline{v} \times \underline{B}$ and $\underline{j} \times \underline{B}$ in terms of the Ohms Law equation which reduces, in this case, to

$$\underline{E} = \frac{1}{ne}\underline{j} \times \underline{B} - \underline{v} \times \underline{B}.$$

These waves are labeled (1) in Fig. 13. The low-frequency Alfven wave comes from the simplest form of Ohms Law

$$\underline{E} + \underline{v} \times \underline{B} = 0.$$

*2) Helicon Waves:* For these waves the ions are considered immobile and electron inertia is neglected ($\omega_{ci} \ll \omega \ll \omega_{ce}$), and the terms $\omega_{ci}/\omega$ and $\omega/\omega_{ce}$ are dropped from (A4). The resulting dispersion relation then acquires the elegantly simple form

$$N^2 = \frac{\omega_{pe}^2}{\omega_{ce}\omega}. \tag{A6}$$

These waves are labeled (2) in Fig. 13, from which the approximation can be seen to be quite accurate in the central region between $\omega_{ci}$ and $\omega_{ce}$. If the right-hand side of (A6) is expanded in terms of plasma parameters

$$N^2 = \left(\frac{c}{V_\phi}\right)^2 = \frac{ne}{\varepsilon_0 \omega B} \tag{A7}$$

and it can be seen that the velocity is independent of the electron or ion mass. The lines of force are helical and rotate carrying the electrons with them, hence the name "helicon waves." Referring back to Ohms Law, these waves are described by the approximate form

$$E = \frac{1}{ne}\underline{j} \times \underline{B}_0.$$

*3) Electron–Cyclotron Wave:* This wave propagates at frequencies below and up to the electron-cyclotron frequency and are labeled (3) in Fig. 13. The ion inertia is neglected and the term $\omega_{ci}/\omega$ disappears from (A4). In ionospheric physics, since the magnetic field is quite low, these waves propagate at frequencies in the audio region and, in general, are heard on receivers as a falling tone. In laboratory plasmas, they propagate as microwaves or radio frequency waves.

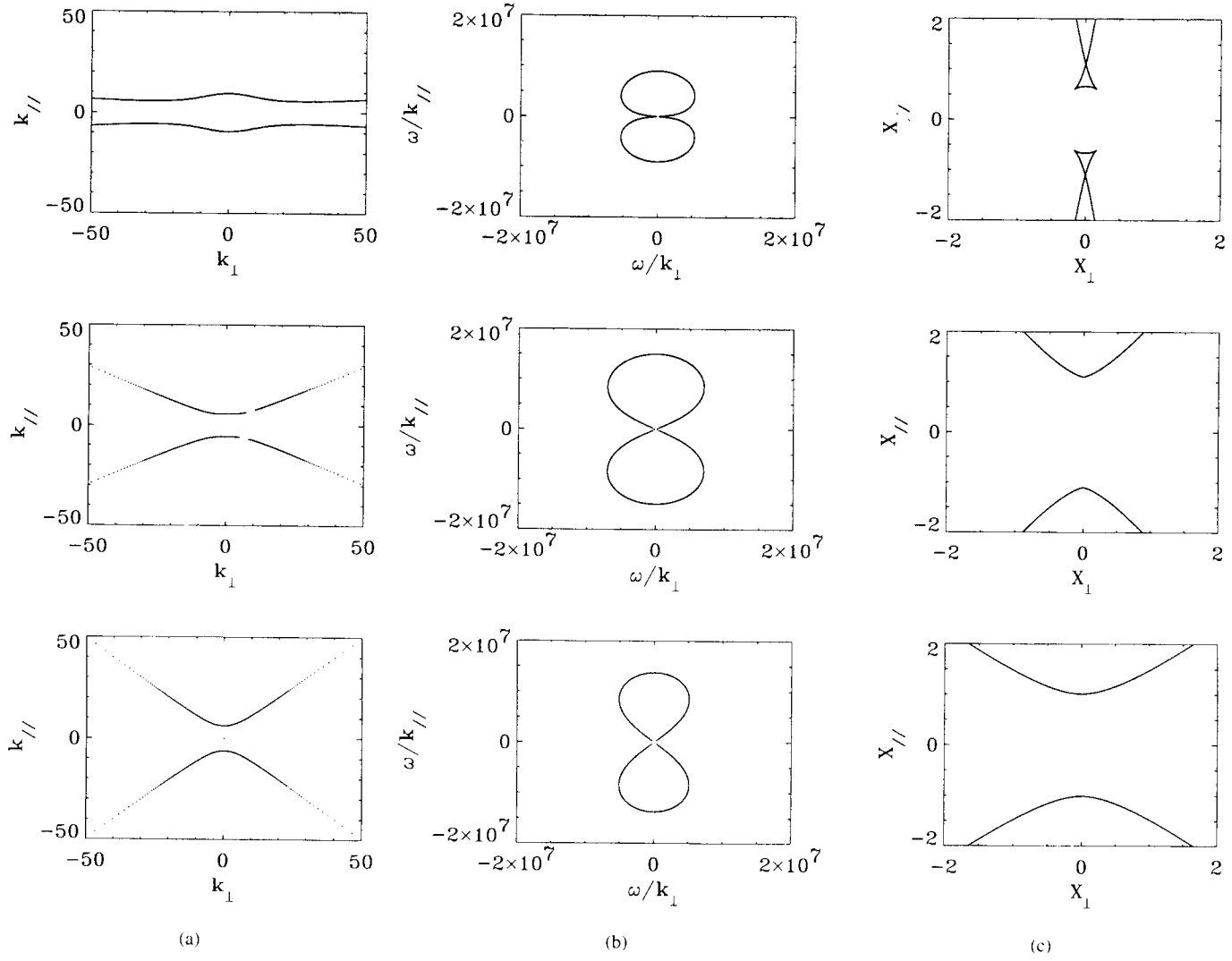


Fig. 14. (a) Refractive index surface, (b) phase velocity (or wave normal) surface, and (c) surfaces of constant phase, all with the vertical axis parallel to the axial magnetic field. The top row is for $\omega/\omega_{ce} = 0.1$; the second row is for $\omega/\omega_{ci} = 0.5$; and the bottom row is for $\omega/\omega_{ci} = 0.7$. For all graphs $\omega_{pi}/\omega_{ci} = 10$.

The dispersion relation is

$$N^2 = \frac{\omega_{pe}^2}{\omega\omega_{ce}\left[1 - \dfrac{\omega}{\omega_{ce}}\right]} \tag{A8}$$

and also describes the propagation of waves in the helicon regime. This is a direct result of the inclusion of the $j \times B_0$ term in Ohms Law, which in this frequency region becomes

$$\underline{E} = \frac{1}{ne}\,\underline{j} \times \underline{B}_0 + \frac{m_e}{ne^2}\,\frac{\partial j}{\partial t}.$$

The only term in Ohms Law which has not been discussed is the term through which the electron inertia manifests itself. If Ohms Law is written for this case

$$E = \frac{m_e}{ne^2}\,\frac{\partial j}{\partial t}$$

and an equation for the perturbing field $\underline{b}$ is formed, it can be seen that this term only describes oscillations at the plasma frequency. However, when the Hall current term $\underline{j} \times \underline{B}$ is linked with the electron inertial term, the electron cyclotron resonance appears. As can be seen from Fig. 13, the electron inertial term has a large effect on the dispersion relation for quite a wide frequency range and will be discussed more fully in a later section. There is a minimum in the refractive index at a frequency $\omega = 0.5\omega_{ce}$ and hence this point marks the maximum phase velocity of the waves.

Finally, we close this section by remarking that the equivalent dielectric tensor can also be used in obtaining the above dispersion relations.

We use the wave equation

$$\nabla \times \nabla \times E = \frac{\omega^2}{c^2}\,\varepsilon.E$$

where the equivalent dielectric tensor $\varepsilon$ is given by

$$\varepsilon = \begin{pmatrix} 1 + \dfrac{\omega_{pe}^2/\omega_{ce}^2}{1-\omega^2/\omega_{ce}^2} & \dfrac{-i\omega_{pe}^2/\omega\omega_{ce}}{1-\omega^2/\omega_{ce}^2} & 0 \\ \dfrac{i\omega_{pe}^2/\omega\omega_{ce}}{1-\omega^2/\omega_{ce}^2} & 1 + \dfrac{\omega_{pe}^2/\omega_{ce}^2}{1-\omega^2/\omega_{ce}^2} & 0 \\ 0 & 0 & 1 - \dfrac{\omega_{pe}^2}{\omega^2} \end{pmatrix} = \begin{pmatrix} \varepsilon_1 & -i\varepsilon_2 & 0 \\ i\varepsilon_2 & \varepsilon_1 & 0 \\ 0 & 0 & \varepsilon_3 \end{pmatrix}. \tag{A9}$$

This approach is equivalent to solving (A1).

### C. Off-Axis Propagation

The full solution for propagation at any angle to the magnetic field shows that the refractive index is severely anisotropic, as can be seen from the simplified Appleton–Hartree relation

$$N^2 = 1 - \frac{\omega_{pe}^2}{\omega(\omega - \omega_{ce}\cos\theta)}. \tag{A10}$$

This has to be taken into account in following a wave as it propagates through an anisotropic plasma, as the phase velocity and group velocity vectors can change in both magnitude and direction. Ray tracing is commonly used in space plasma physics and wave propagation in large toroidal plasmas used for fusion research. Since typical helicon sources are cylindrical and the wave is constrained by density gradients and the physical boundaries of the vacuum system, it is important to understand the basic physics of wave propagation in an anisotropic medium.

Although the general principles are given in a number of texts, we have chosen Stix [45, ch. 3, and references therein] as the basis for the following review.

Group velocity has always been a difficult concept involving forerunners at the velocity of light and a slower velocity associated with modulation or interference. One tends to think of varying frequencies in these cases; however, in that which follows, we consider a point antenna emitting a fixed frequency, and a wave number ($k$) which varies with the anisotropy of the refractive index using the definition of group velocity $v_g = \partial\omega/\partial k$.

It was only in the early 1950's that contemporaries of Storey [5] showed that in a medium such as the anisotropic plasma considered here, the group velocity vector had a magnitude and direction equal to the Pointing vector, i.e., the energy of the wave moved with the group velocity along the ray direction.

Commonly, the anisotropic nature of the plasma is shown as a polar plot of $N$ versus $\theta$ where $\theta$ is the angle relative to the steady magnetic field. Three examples are given in Fig. 14(a) where (A10) is used to plot $N$ as a function of $\theta$, for $\omega/\omega_{ce}$ equal to 0.7, 0.5, and 0.1 with $\omega_{pe}/\omega_{ce} = 10$. The existence of the $\cos\theta$ in the denominator of (A10) results in the curves approaching an asymptote given by $\cos\theta = \omega/\omega_{ce}$ (for $\omega_{pe} \gg \omega_{ce}$).

The ray direction is given by the normal to the $N$, $\theta$ surface. It is not simple to use this surface to obtain the radiation pattern from a point source and the phase velocity surface (or wave normal surface), which is reciprocal to the $N$, $\theta$ surface, is normally used. The surfaces resulting from the inversion corresponding to Fig. 14(a) are shown in Fig. 14(b). Now the surfaces are closed but the angle of the asymptote remains unchanged. If we imagine the origin as a point source radiating waves with a frequency $\omega$, all the phase velocity vectors will be contained within a cone of opening angle $\theta$ centered on the direction of the magnetic field $B_0$. This is called the phase velocity resonance cone ($RC_\phi$).

To obtain the radiation pattern, we need to return to configuration space (the laboratory frame) and trace out the ray surface which is really a snapshot of the surfaces of constant phase (SCP). Following Stix [45], the ray surface can be constructed geometrically from the wave normal surface by drawing phase velocity vectors from the origin in Fig. 14(b) out to the wave normal surface. At the tip of the phase velocity vector, a perpendicular line is constructed which represents a particular wavefront that has propagated from the origin in unit time. If this is done for all angles from zero (parallel to $B_0$) to the $RC_\phi$ angle, the intersection of all the perpendiculars will form the ray surface [Fig. 14(c)]. Essentially, this surface represents the points of constructive interference of all possible wave fronts which have propagated from the origin in unit time.

Once again, a resonance cone appears, but this time at an angle complimentary to the phase velocity resonance cone. Here, the surfaces of constant phase are open and approach a group velocity resonance cone ($RC_g$) defined by $\sin\theta = \omega/\omega_{ce}$ (for $\omega_{pe} \gg \omega_{ce}$).

One could ask how open-ended surfaces of constant phase can physically occur; the answer lies in the understanding of the group velocity. Normally, only the slow velocity associated with the propagation of a wave packet is considered, and it is this we have used in the development of the ray surfaces. The forerunners mentioned earlier, which propagate at the speed of light, move out in front and serve to close the ray surfaces; their amplitude is small and generally they are not seen in experiments which are not pulsed.

The first thing to be noticed from Fig. 14 is that although the phase velocity surfaces look very similar, the refractive index and surface of constant phase diagrams change dramatically as the frequency is increased from 0.1–0.7 $\omega_{ce}$. For high frequencies, the $RC_g$ opens out yielding the broad smooth SCP seen for 0.7 $\omega_{ce}$.

Close inspection of the SCP for 0.5 $\omega_{ce}$ shows a corner at $\theta = 0$ which arises from the flattening of the $N$, $\theta$ surface for $\theta$ less than 20 to 30°. In fact, the whole propagation characteristic changes at this frequency where, as noted previously, the parallel phase velocity has a maximum. This arises because the Hall term is starting to dominate over the electron inertia. We can also note that $k$ vectors in this angular region all have a group velocity which is nearly parallel to the magnetic field (the group velocity direction being given by the normal to the refractive index surface) which will tend to guide the

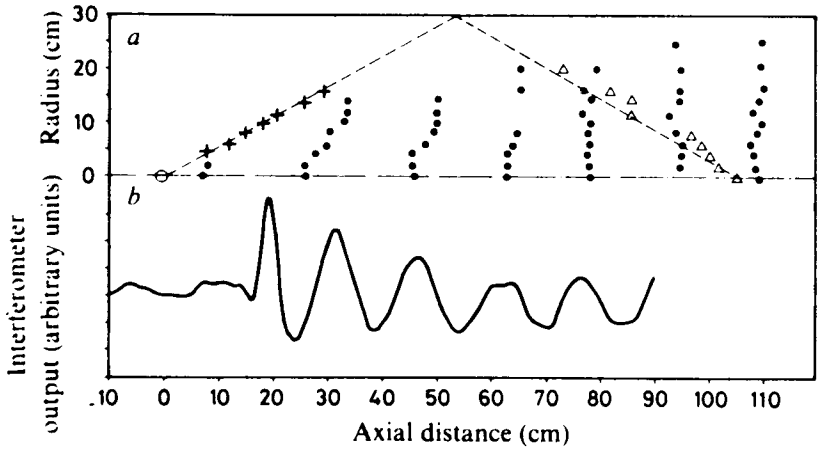


Fig. 15. Radiation pattern from a small-loop antenna in a large magneto plasma showing the surfaces of constant phase and the resonance cone propagating away from the antenna and reflecting from the chamber wall. Experimental conditions are plasma density = $4 \times 10^{10}$ cm$^{-3}$, $B_0 = 64$ G, $\omega/\omega_{ce} = 0.47$, and argon pressure = $4 \times 10^{-4}$ mTorr. (Reprinted from [47].)

wave along the magnetic field. Below 0.5 $\omega_{ce}$, the corner in the SCP resolves itself into two cusps which for lower frequencies define the maximum angle of 19.28° [5] at which the wave can propagate.

The cusps in the SCP for 0.1 $\omega_{ce}$ correspond to the inflection points in the $N$, $\theta$ surface.

As the frequency decreases even further, the RC$_o$'s approach 90° and the dispersion is more and more determined by the Hall term, i.e., the wave becomes more electromagnetic and less electrostatic. Finally, we note that the SCP joining the two cusps arises essentially from the Hall term, and its propagation characteristics will mimic very closely those of an infinite plane-wave propagating parallel to the magnetic field. That part of the SCP extending from the cusp to the resonance cone results from the increasing refractive index caused by the electron inertia.

The resonance cones were first studied by Fisher and Gould [46] who clearly showed that, in the lab frame, it is the group velocity resonance cone which is observed and not the phase velocity resonance cone thereby resolving a considerable controversy. These experiments were carried out in low-density plasmas where the parallel wavelength was much longer than the machine dimension, hence, only the fields of the resonance cone were detected. When the density is increased, the parallel wavelength decreases and the surfaces of constant phase can be measured along with the resonance cone.

The first measurements of both these phenomena were made in the mid 1970's [47], [48] and a single reflection of the resonance cone from the cylindrical walls of the vacuum chamber can be seen in Fig. 15. In this experiment, a 1-cm-diameter loop excited the waves on the axis of a large cylindrical plasma. The SCP are marked by the solid circles, the RC$_g$ propagating directly from the antenna by the crosses and the reflected RC$_g$ by the triangles. About a meter away from the antenna, it seems that we have two rather different waves in the system—the first is the mainly electromagnetic whistler and the other is an electrostatic wave with an axial wavelength defined by the RC$_g$ and the point of reflection (in this case the walls of the cylinder) which leads to a potential maximum at the axial position where all the reflections of the RC$_g$ meet.

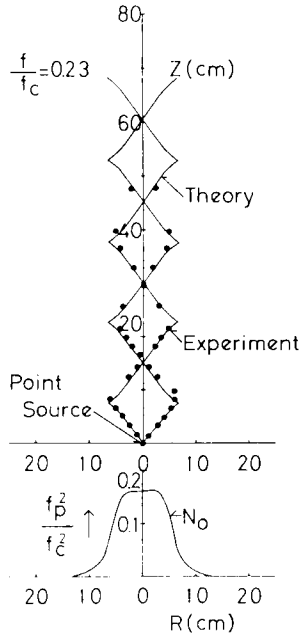


Fig. 16. Multiple reflections of the resonance cone which give rise to the TG modes in the same apparatus as Fig. 15 with similar experimental conditions. (Reprinted from [49].)

Multiple reflections of the RC$_g$ in the same system were reported later [49] and showed very good agreement with theory. In this case, the radial plasma density was defined by an aperture plate having a diameter of about 10 cm and the RC$_g$ reflected off the density gradient as can be seen in Fig. 16.

At about the same time [50], Gonfolone clearly showed multiple reflections of RG$_g$ in an afterglow plasma. As the plasma density decreased, $\omega_{pe}$ became less than $\omega_{ce}$ and the resonance cone angle became inversely dependent on $\omega_{pe}$ producing interfering reflections which decreased in length along the axis of the plasma. Using the complete formula for

the group velocity resonance cone [4]

$$\sin^2\theta = \omega^2\left(\omega_{pe}^2 + \omega_{ce}^2 - \omega^2\right)/\omega_{pe}^2\omega_{ce}^2$$

and introducing the plasma radius $a$, and a wavelength $\lambda$ defined by the distance between interference maxima along the axis caused by the reflected interfering resonance cones, simple geometric relations were used to determine a dispersion relation

$$ka = \pi\left[\omega^2\left(\omega_{pe}^2 + \omega_{ce}^2 - \omega^2\right)/\left(\omega_{ce}^2 - \omega^2\right)\left(\omega_{pe}^2 - \omega^2\right)\right]^{1/2}. \tag{A11}$$

In a private communication Leuterer (at that time at the Max Planck Institute in Garching) noted the similarity between these interference maxima and electrostatic wave modes in a plasma cylinder of radius $a$, which had been reported previously [51]. The latter are commonly called Trivelpiece–Gould (TG) modes and their dispersion relation is

$$ka = p_{n\nu}\left[\omega^2\left(\omega_{pe}^2 + \omega_{ce}^2 - \omega^2\right)/\left(\omega_{ce}^2 - \omega^2\right)\left(\omega_{pe}^2 - \omega^2\right)\right]^{1/2} \tag{A12}$$

where $p$ is the $\nu$th order Bessel function. The similarity between the two dispersion relations is striking, and it is reasonable to suggest that the TG modes can be thought of as arising from wave vectors near the resonance cone.

By using the equivalent dielectric tensor, some more light can be thrown on the relationship between the TG modes and the helicons. As the TG modes are electrostatic, they have a dispersion relation given by

$$k.\varepsilon.k = 0$$

where $\varepsilon$ is given by (A9). This leads to the result

$$\varepsilon_1 k_\perp^2 + \varepsilon_3 k_z^2 = 0$$

where $k_\perp$ is the perpendicular wave number and $k_z$ is the parallel wave number. Substituting the expressions for $\varepsilon_1$ and $\varepsilon_3$ leads to the dispersion relation for the TG mode

$$\frac{k_\perp^2}{k_z^2} = \frac{\omega^2\left(\omega_{pe}^2 + \omega_{ce}^2 - \omega^2\right)}{\left(\omega_{ce}^2 - \omega^2\right)\left(\omega_{pe}^2 - \omega^2\right)}. \tag{A13}$$

This expression is also the helicon dispersion relation with finite electron inertia as $k_\perp \to \infty$, thus for high values of $k_\perp$, the helicon wave becomes electrostatic and is, in essence, a TG mode.

This will be discussed more fully in the section dealing with the effect of electron inertia in a cylindrical geometry. A fairly comprehensive review of the theory and experimental evidence for radiation of whistler-mode waves from a point source in a cylindrical plasma has been published by Ohnuma [7].

### *D. Propagation in Cylindrical Geometry*

The most comprehensive treatment of cylindrically confined helicons was carried out by KMT [11] in 1965 and their analysis is reviewed below.

They start from (A1) and omit the $v \times B_0$ term while including the resistivity to obtain

$$\underline{E} = \frac{1}{ne}\,\underline{j} \times \underline{B}_0 + \frac{m_e}{ne^2}\frac{\partial j}{\partial t} + \eta j. \tag{A14}$$

Along with Maxwell's equations and neglecting the displacement current, two equations for the perturbation quantities are obtained

$$\begin{aligned} \text{curl } b &= \mu_0 j \\ \text{curl } E &= -\delta b/\delta t \end{aligned} \tag{A15}$$

which are to be solved for pertubations $b = b(r)\exp[i(m\theta + kz - \omega t)]$.

The plasma fields are combinations of Bessel functions, e.g.,

$$b_z(r) = A_1 J_m(\gamma_1 r) + A_2 J_m(\gamma_2 r). \tag{A16}$$

For an insulating boundary, Maxwell's equations are solved for a vacuum yielding fields of the form

$$b_z(r) = ikA_3 K_m(kr) \tag{A17}$$

where $J_m$ is a Bessel function of the first kind, $K_m$ is a McDonald function, the $A$'s are arbitrary constants, and the $\gamma$'s are radial wave numbers.

By applying boundary conditions for the continuity of the wave magnetic fields across the boundary (i.e., no infinite surface currents), the arbitrary constants may be eliminated and a determinental equation arrived at which is the dispersion relation. This was solved numerically for $m = 0, +1$, and $-1$ azimuthal modes and plotted for a variety of plasma densities, magnetic fields, and collision frequencies. They note that for very low values of $\omega_{ce}\tau$ (which they use as a resistivity parameter), the wave fields became more concentrated at the boundary giving rise to a skin field. This rather curious form of surface wave is linked to the TG modes mentioned earlier.

For plasmas surrounded by a conducting cylinder, the boundary conditions are simply that the tangential components of the electric field at the boundary should be zero [22], [52] and the dispersion relation reduces to the relatively simple determinental equation

$$\begin{vmatrix} \gamma_1 J_m(\gamma_1 a) & \gamma_2 J_m(\gamma_2 a) \\ \dfrac{m}{\gamma_1 a} J_m(\gamma_1 a) + \dfrac{k}{q_1} J_m(\gamma_1 a) & \dfrac{m}{\gamma_2 a} J_m(\gamma_2 a) + \dfrac{k}{q_2} J_m(\gamma_2 a) \end{vmatrix} = 0 \tag{A18}$$

where the wave vector $q^2 = (N\omega/c)^2 = k^2 + \gamma^2$ and is obtained from the plane-wave dispersion relation (A10), and $\gamma$ and $k$ can be considered as radial and longitudinal wave numbers, respectively. Since (A10) is quadratic, there are two values for $q$ and, hence, two values for $\gamma$ denoted by the subscripts 1 and 2.

The reaction of the wave propagation to radial nonuniformities in the plasma density was also investigated [22]. They found that while the inclusion of cylindrical boundaries served to decrease $k$ (increase the axial wavelength) over the case of an infinite plane-wave propagating parallel to $B_0$ , increasing degrees of radial nonuniformity tended to increase $k$, even to the extent of having $k$ greater than the infinite plane-wave case! Fig. 17 shows the different dispersion for the infinite plane-wave propagating parallel to $B_0$ and waves propagating in cylinders with conducting and insulating boundaries.

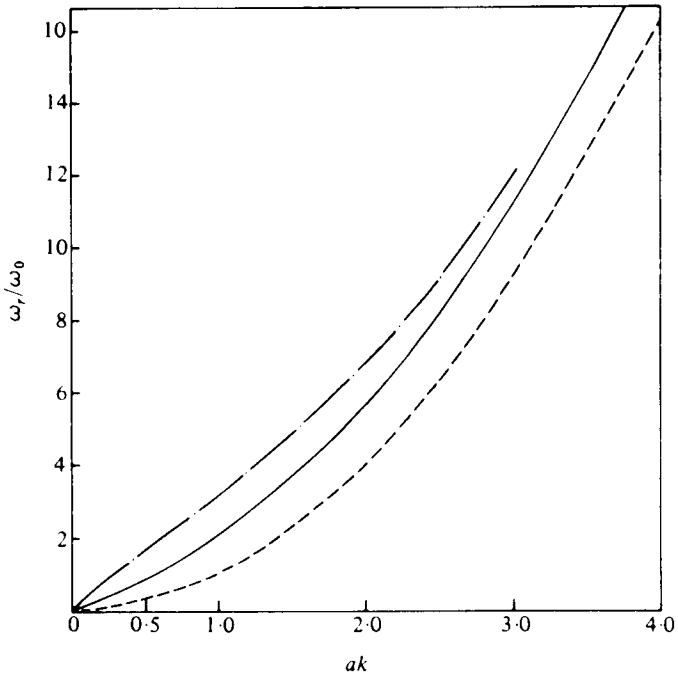


Fig. 17. Whistler (Helicon) dispersion for—— rigid nonconducting boundaries, – – – conducting boundaries, and - - - - infinite plane-wave propagating parallel to $B_0$. The effect of the different boundaries becomes important when $a$ and $k$ are comparable.

### *E. The Effects of Electron Inertia*

In the 1960's there was a debate as to whether it was necessary to include the electron inertia in the dispersion of helicons. It was known that there was a relation between the helicon solutions and the TG modes [53] and that although both modes could propagate in a magnetized plasma cylinder, their dispersion was quite different. It was pointed out that higher order radial wave-mode numbers tended to decrease $k$, and a simple approximation was given for their dispersion.

The dispersion relation (A18) has been used [23] to show that the electron inertia had a measurable effect on the dispersion of the waves for frequencies at least as low as 0.1 $\omega_{ce}$ and the result verified by experiment.

There are an infinity of solutions to these eigenvalue problems, and generally the higher order modes are ignored on the premise that they are highly damped. This is not necessarily the case for all experimental conditions.

In searching for solutions of the cylindrical dispersion relation which could be fitted to the experimental points, Boswell [54] found that higher order radial modes were strongly affected by the electron inertia. By plotting the parallel wave number against the radial-mode number, he showed that although the dispersion neglecting electron inertia was reasonably correct for $n = 1$, for higher $n$ numbers, major discrepancies appeared for higher values with the dispersion approaching an asymptote given by

$$ak = (\omega/\omega_{ce})n\pi \tag{A19}$$

where $a$ is the cylinder radius and $n$ the radial-mode number. This curious behavior was not further investigated for some time.

In the early 1980's the effect of the boundary conditions on the radial-mode structure was revisited [55] and by approximating the radial eigenmode spacing by $\gamma a = \pi$, it was shown that the asymptote (A19) was simply the resonance cone angle discussed in (A3).

This is shown in Fig. 18 where for this example we have taken $\omega/\omega_{ce} = 0.1$ and $\omega_{ce}/\omega_0 = 40$ ($\omega_0 = \omega_{ce}c^2/\omega_{pe}^2a^2$), conditions which correspond approximately to the WOMBAT experiment with $a = 10$ cm, $B_0 = 50$ G, and $n_e \sim 10^{11}$ cm$^{-3}$. The parameter $\omega_0$ appears in the helicon dispersion since it is proportional to $B_0/n_e$ which is proportional to the square of $\lambda$ in the infinite plane-wave dispersion. In Fig. 18, the axial wave number for radial modes up to $n = 8$ are plotted for the $m = 1$ azimuthal mode with conducting boundary conditions. On the same figure is plotted the angular dependence of the plane-wave dispersion for the same conditions. It should be noted that although $k$ is plotted against $\gamma$, this is equivalent to plotting the refractive index surface since $N = c/V_\phi = kc/\omega$ and so, for constant $\omega$, the two surfaces are identical save for a multiplicative factor $c/\omega$. The curve 1 in Fig. 18 is derived by simply using the electron inertia neglecting the Hall term, curve 2 by including the Hall term and neglecting electron inertia, and curve (3) by including both. To allow everything to be presented on the same graph, the radial eigenmode spacing has been approximated as $\gamma a = \pi$. Clearly, the dispersion of the radial modes follows the refractive index surface.

The phase velocity resonance cone is very evident in curve 1 and has an angle $\theta = \arccos(\omega/\omega_{ce}) = \arccos(0.1) = 84°$. Curve 2 is the helicon approximation for which (for $B_0$ constant) $k\alpha\omega_{pe}\alpha(n_e)^{1/2}$ and for very large $n_e$ will dominate over curve (1) for propagation angles close to $B_0$, for which the helicon approximation is adequate in describing the dispersion of the lowest order radial mode. However, for higher order modes, the electron inertia begins to dominate over the Hall term (even allowing two modes to propagate with the same $k$), and the modes asymptotically approach RC$_\phi$. As $\omega$ nears $\omega_{ce}$, the electron inertia dominates the dispersion, which is only weakly affected by $n_e$. For frequencies far from $\omega_{ce}$, the RC$_\phi$ angle approaches $\pi/2$ and the electron inertia plays essentially no role in the dispersion of the modes.

As discussed earlier, the reflections of the group velocity resonance cone from the boundaries will form the basic structure of the TG modes, although their dispersion will be determined by the phase velocity resonance cone. For the conditions of Fig. 18, the first radial mode is mainly electromagnetic and the TG mode associated with the reflected resonance cones will have a value of $ka$ about ten times smaller. Hence in an experiment, one would expect to measure an interference between an electromagnetic (EM) wave, and an electrostatic (ES) wave having a wavelength about ten times longer. The wave vector becomes more perpendicular as the radial-mode number increases and the dispersion becomes dominated by the resonance cone, i.e., the wave becomes electrostatic in character.

It is now clear that the resonance cones incorporate the higher order radial modes of the TG waves. At high $k_\perp$, the helicon dispersion relation simplifies to that associated with the TG mode $k_z = \gamma k_\perp$, where $\gamma$ is the angle of the RC$_g$. An

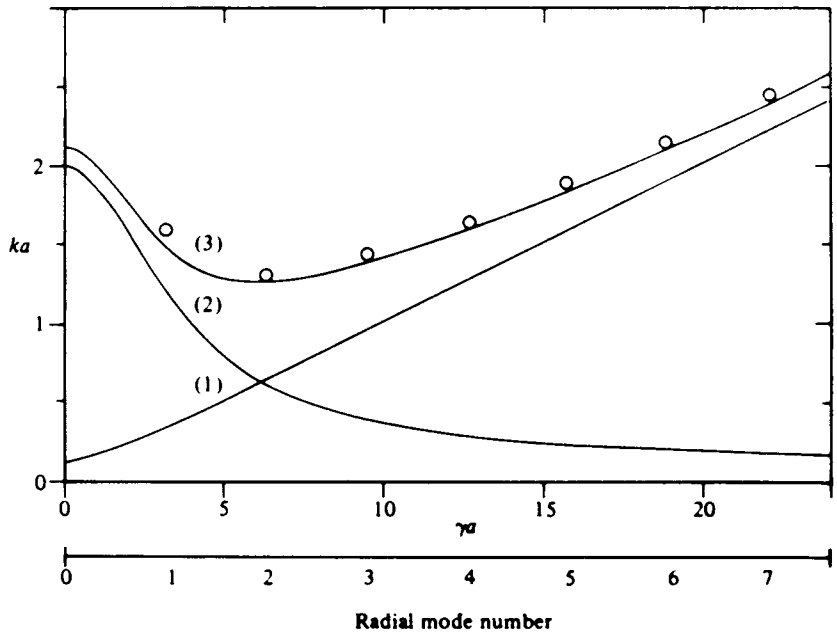


Fig. 18. Radial eigen modes (open circles) and plane-wave solutions for whistlers with $\omega/\omega_{ce} = 0$, 1 and $\omega/\omega_0 = 40$. Curve 3 is the full dispersion, curve 2 is neglecting electron inertia, and curve 1 is neglecting the Hall term. The radial eigenmode spacing has been approximated as $\gamma a = \pi$. (Reprinted from [55].)

antenna located in the $x$–$y$ plane (perpendicular to $B_0$ which lies along the $z$ axis) with a charge density $\rho = \exp(ik_y y)\delta(z)$ excites a TG mode where the wavefronts lie along $k_z = \gamma k_y$ and the direction of propagation of the mode is that of the $RC_\phi$. The fine structure of the resonance cone (the higher order radial modes) is produced by the high $k_y$ components of the antenna. In a two-dimensional waveguide with a conducting boundary, the boundary conditions at the walls are satisfied by a set of image sources located outside the guide which can then produce the modes seen in the eigenmode analysis.

In summary, we can say that the effect of the electron inertia is to introduce an ES component to the wave fields, which in cylindrical geometry appear as TG modes of varying radial complexity. For high $n_e$ and low $B_0$, the wave is predominantly EM and its dispersion is governed by the Hall term. This would be called the classic helicon wave. For high magnetic fields, low densities or frequencies close to $\omega_{ce}$, the electron inertia dominates and the wave will have strong ES characteristics. Experimentally it will be the wave with the shortest $\lambda$ and the EM wave having a very long $\lambda$, generally much longer than the plasma. It should be noted that the propagation of the ES waves in a plasma with a finite electron temperature will be strongly influenced by Landau damping since their wavelength can be quite small and their phase velocity can be close to the thermal velocity of the electrons.

The EM wave will suffer collisionless damping only close to $\omega_{ce}$ where electrons moving opposite to the wave phase velocity will see the wave-frequency doppler shifted to $\omega_{ce}$ and take energy from the perpendicular component of the wave field.

Although these waves seem to be separate entities, they are a result of the anisotropic nature of the refractive index and are part of the dispersion of the same wave propagating at different angles in a cylinder.

## ACKNOWLEDGMENT

The authors would like to thank Prof. S. M. Hamberger, Dr. D. Henry, Prof. H. A. Blevin, Dr. P. J. Christiansen, and Prof. A. Bouchoule for their positive encouragement. They would also like to thank Prof. Leon Shohet for suggesting that the two authors collaborate on their project. Until 1984, all the funding had come from sparse university resources. Subsequently, most of the development was carried out on external contracts. For figures reprinted in this paper, the authors would like to acknowledge the following journals: *Journal of Geophysical Research*, *Physical Review Letters*, *Proceedings of the Physical Society*, *Plasma Physics and Controlled Fusion*, *Journal of Plasma Physics Nature*, and IEEE TRANSACTIONS ON PLASMA SCIENCE.

## REFERENCES

[1] H. Barkhausen, "Whistling tones from the earth," *Proc. I.R.E.*, vol. 18, p. 143, 1930.
[2] D. R. Hartree, "The propagation of electromagnetic waves in a refracting medium in a magnetic field," *Proc. Cambridge Phil. Soc.*, vol. 27, p. 143, 1931.
[3] E. V. Appleton, "Wireless studies of the ionosphere," *J. Inst. Elec. Engrs.*, vol. 71, p. 642, 1932.
[4] H. G. Booker, "Propagation of wave-packets incident obliquely upon a stratified doubly refracting ionosphere," *Philos. Trans. R. Soc. London A, Math. Phys. Sci.*, vol. 237A, p. 411, 1938.
[5] L. R. Storey, "An investigation of whistling atmospherics," *Philos. Trans. R. Soc. London A, Math. Phys. Sci.*, vol. 246, p. 113, 1953.
[6] L. D. Landau, "On the vibrations of the electronic plasma," *J. Phys.*, vol. 10, p. 25, 1946.
[7] J. M. Dawson, "Nonlinear electron oscillations in a cold plasma," *Phys. Rev.*, vol. 113, p. 383, 1959.
[8] P. Aigrain, "Les 'helicons' dans les semiconducteurs," in *Proc. Int. Conf. Semiconductor Physics*, Prague, Czeckoslovakia, 1960, p. 224.
[9] F. E. Rose, M. T. Taylor, and R. Bowers, "Low frequency magneto plasma resonances in sodium," *Phys. Rev.*, vol. 127, p. 1122, 1962.
[10] C. R. Legéndy, "Macroscopic theory of helicons," *Phys. Rev.*, vol. 135, p. 1713, 1965.
[11] J. P. Klosenberg, B. McNamara, and P. C. Thonemann, "The dispersion and attenuation of helicon waves in a uniform cylindrical plasma," *J. Fluid Mech.*, vol. 21, p. 545, 1965.

[12] G. N. Harding and P. C. Thonemann, "A study of helicon waves in indium," *Proc. Phys. Soc.*, vol. 85, p. 317, 1965.
[13] T. A. Facey and G. N. Harding, Culham Laboratory, Rep. CLM-R66, 1966.
[14] R. M. Gallet, J. M. Richardson, B. Wieder, and G. D. Ward, "Microwave whistler mode propagation in a dense laboratory plasma," *Phys. Rev. Lett.*, vol. 4, p. 347, 1960.
[15] H. A. Blevin and P. C. Thonemann, Culham Laboratory, Rep. CLM-R12, 1961.
[16] J. A. Lehane and P. C. Thonemann, "An experimental study of helicon wave propagation in a gaseous plasma," *Proc. Phys. Soc.*, vol. 85, p. 301, 1965.
[17] V. V. Chechin, M. P. Vasil'ev, L. I. Guigor'eva, A. V. Longinov, and B. I. Smerdov, *J.E.T.P. Lett.*, vol. 2, p. 260, 1965.
[18] M. P. Vasil'ev, L. I. Gregor'eva, A. V. Longinov, B. I. Smerdov, and U. U. Chechkin, "Plasma heating by a fast magnetosonic wave of large amplitude," *J.E.T.P.*, vol. 27, p. 882, 1968.
[19] V. D. Shafranov, *J.E.T.P.*, vol. 34, p. 1019, 1958.
[20] H. A. Blevin, J. A. Reynolds, and P. C. Thonemann, Culham Laboratory, Rep. CLM P204, 1969.
[21] A. N. Kondratenko, "Kinetic theory of electromagnetic waves in a bounded magnetoplasma," *Sov. Phys. Tech Phys.*, vol. 11, p. 590, 1966.
[22] H. A. Blevin and P. J. Christiansen, "Propagation of helicon waves in a nonuniform plasma," *Aust. J. Phys.*, vol. 19, p. 501, 1966.
[23] H. A. Blevin, P. J. Christiansen, and B. Davies, "Effect of electron cyclotron resonance on helicon waves," *Phys. Lett. A*, vol. 28, p. 230, 1968.
[24] B. Davies, "Helicon wave propagation: Effect of electron inertia," *Phys. Rev. Lett.*, vol. 22, p. 1246, 1969.
[25] A. B. Jolly, G. Martelli, and J. F. Troughton, "Helicon wave propagation in a laboratory plasma," *Plasma Phys.*, vol. 10, p. 863, 1969.
[26] R. W. Boswell, "Modulated RF produced argon magneto-plasma," School of Physical Sciences, The Flinders University of South Australia, Internal Rep. PR 68/8, 1968.
[27] ———, "Plasma production using a standing helicon wave," *Phys. Lett.*, vol. 33A, pp. 457–458, 1970.
[28] ———, "Very efficient plasma generation by whistler waves near the lower hybrid frequency," *Plasma Phys. Control Fusion*, vol. 10, pp. 1147–1162, 1984.
[29] V. D. Shrafranov, *J.E.T.P.*, vol. 34, p. 1475, 1958.
[30] V. V. Dolgopolov, A. I. Ermankov, N. I. Nazarov, K. N. Stepanov, and V. T. Tolok, "Cerenkov absorption of 'whistles' in an inhomogeneous plasma cylinder," *Nucl. Fusion*, vol. 3, p. 251, 1963.
[31] H. Oechsner, "On the influence of superimposed DC magnetic fields on the density of electrodeless HF plasmas," in 1970 *Int. Conf. on Gas Discharges*, p. 187.
[32] ———, "Electron cyclotron wave resonances and power absorption effects in electrodeless low pressure HF plasmas with superimposed static magnetic field," *Plasma Phys. Control Fusion*, vol. 16, p. 835, 1973.
[33] E. P. Szuszczewicz and H. Oechsner, "Spatial distribution of plasma density in a high-frequency discharge with a superimposed static magnetic field," *Phys. Fluids*, vol. 15, p. 2240, 1972.
[34] S. O. Knox, F. J. Paoloni, and Kristiansen, "Helical antenna for exciting azimuthally asymmetric Alfven waves," *M. J. Appl. Phys.*, vol. 46, p. 2516, 1975.
[35] G. Lisatano, R. A. Ellis, W. M. Hooke, and T. H. Stix, "Production of a quiescent discharge with high electron temperature," *Rev. Sci. Instrum.*, vol. 39, p. 295, 1968.
[36] T. Watari, T. Hatori, R. Kumasawa, S. Hidekuma, T. Aoki, T. Kawamoto, W. Inutake, S. Hiroe, A. Nishizawa, K. Adati, T. Sato, T. Watanabe, H. Obayashi, and K. Takayama, "Radio-frequency plugging of a high density plasma," *Phys. Fluids*, vol. 21, p. 2076, 1978.
[37] R. W. Boswell, "A study of waves in gaseous plasmas," Ph.D. thesis, Flinders Univ. of S. Australia, 1974.
[38] T. Shoji, "Experiment on RF plasma production in CHS," *Annu. Review*, Institute of Plasma Physics, Nagoya Univ., Japan, 1986, p. 67.
[39] Nagoya publication.
[40] R. W. Boswell, R. K. Porteous, A. Prytz, and A. Bouchoule, "Some features of RF excited fully ionized low pressure argon plasma," *Phys. Letts. A*, vol. 91, p. 163, 1982.
[41] R. W. Boswell and D. Henry, "Pulsed high rate plasma etching with variable $Si/SiO_2$ selectivity and variable Si etch profiles," *Appl. Phys. Lett.*, vol. 47, p. 1095, 1985.
[42] R. W. Boswell, "Method and apparatus for producing a high density magneto-plasma," Australian Patent 58606/86, and most other countries.
[43] L. Spitzer, "Physics of fully ionized gases," in *Interscience*, 2nd ed. New York: McGraw-Hill, 1962.
[44] P. J. Christiansen, "Experimental study of helicon waves," Ph.D. thesis, Flinders Univ. of S. Australia, 1969.
[45] T. H. Stix, *The Theory of Plasma Waves*. New York: McGraw-Hill, 1962, ch. 3 and references therein.
[46] R. K. Fisher and R. W. Gould, "Resonance cones in the field pattern of a radio frequency probe in a warm anisotropic plasma," *Phys. Fluids*, vol. 14, p. 875, 1971.
[47] R. W. Boswell, "Measurements of the far field resonance cone for whistler mode waves in the magnetoplasma," *Nature*, vol. 58, p. 258, 1975.
[48] R. L. Stenzel, *Radio Sci.*, vol. 11, p. 1045, 1976.
[49] T. Ohnuma, "Radiation phenomena of plasma waves," *IEEE Trans. Plasma Sci.*, vol. PS-6, p. 464, 1978.
[50] A. Gonfolone, "Reflection of resonance cone and plasma-filled waveguide modes," *Appl. Phys. Lett.*, vol. 32, p. 530, 1978.
[51] A. W. Trivelpiece and R. W. Gould, "Space charge waves in cylindrical plasma columns," *J. Appl. Phys.*, vol. 30, p. 1784, 1959.
[52] B. Davies, "Helicon wave propagation: Effect of electron inertia," *J. Plasma Phys.*, vol. 4, p. 43, 1970.
[53] R. L. Ferrari and J. P. Klozenberg, "The dispersion and attenuation of helicon waves in a cylindrical plasma-filled waveguide," *J. Plasma Phys.*, vol. 2, p. 283, 1968.
[54] R. W. Boswell "Dependence of helicon wave radial structure on electron inertia," *Aust. J. Phys.*, vol. 25, p. 403, 1972.
[55] R. W. Boswell, "Electrostatic and electromagnetic eigen modes near the electron and ion gyrofrequencies in a cylindrical plasma," *J. Plasma Phys.*, vol. 31, p. 197, 1984.

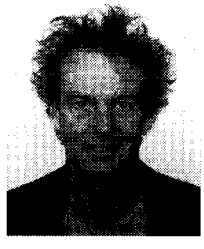

**Rod W. Boswell** has been working at the Australian National University in Canberra since 1980. His interests include helicon plasmas and particles in cell simulation.

**Francis F. Chen** has had a 43-year career in plasma physics which includes contributions to probe diagnostics, resistive drift waves, magnetic and inertial fusion, laser-plasma interactions, laser accelerators, and gas discharges. His recent interest in industrial applications led to the present work on helicon sources. He has also authored a popular textbook.

Mr. Chen won the IEEE Plasma Science and Applications Award and the APS Maxwell Prize.